Macromolecules

Article

pubs.acs.org/Macromolecules

Synthesis and Crystallinity of Conjugated Block Copolymers Prepared by Click Chemistry

Kendall A. Smith,[†] Yen-Hao Lin,[†] Dana B. Dement,[†] Joseph Strzalka,[‡] Seth B. Darling,[§,∥] Deanna L. Pickel,[⊥] and Rafael Verduzco*[,†]

[†]Department of Chemical and Biomolecular Engineering, Rice University, MS-362, 6100 Main Street, Houston, Texas 77005-1892, United States

[‡]X-ray Science Division, Argonne National Laboratory, Argonne, Illinois 60439, United States

[§]Center for Nanoscale Materials, Argonne National Laboratory, Argonne, Illinois 60439, United States

[∥]Institute for Molecular Engineering, The University of Chicago, Chicago, Illinois 60637, United States

[⊥]Center for Nanophase Materials Sciences, Oak Ridge National Laboratory, Oak Ridge, Tennessee 37831, United States

Supporting Information

ABSTRACT: Conjugated block copolymers have the potential to improve solution processed optoelectronic devices such as organic photovoltaics (OPVs), but significant synthetic challenges exist and systematic studies investigating structure–property relationships are lacking. We demonstrate a new route to conjugated block copolymers via copper-catalyzed click coupling and apply this method to synthesize a series of poly(3-hexylthiophene)-*block*-poly(9,9-dioctylfluorene) (P3HT-*b*-PF) conjugated block copolymers with varying block weight fractions. The resulting block copolymers are comprised of two conjugated polymers joined by a flexible, nonconjugated linker. The series of conjugated block copolymers prepared enables an investigation into the role of polymer block lengths and composition on crystallization and self-assembly behavior. Grazing incidence wide-angle X-ray scattering measurements indicate the formation of highly oriented P3HT and/or PF crystallites in thermally annealed block copolymer films. Crystallization of either P3HT or PF blocks is predominant in all block copolymers studied, but at intermediate ratios crystallization of both blocks is observed.

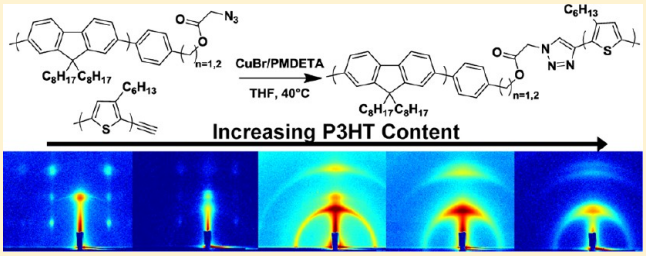

INTRODUCTION

Conjugated polymers are solution-processable materials that can serve as key components in organic electronic devices, including bulk-heterojunction organic photovoltaics (OPVs), organic thin-film transistors, and organic light-emitting diodes.[1−3] Significant effort has been devoted to understanding and directing their mesoscale and nanoscale structure in order to optimize their optoelectronic properties for use in organic electronic materials and devices.[4−8] Conjugated block copolymers contain two or more conjugated polymer blocks and may enable simplified approaches to controlling the microstructure of conjugated polymer thin films.[9−13] These materials can potentially prevent large-scale phase separation in organic semiconductor blends and define thermodynamically stable nanostructures through microphase segregation, providing a path to optimal active layer structures for bulk heterojunction OPVs with good long-term stability. Donor–acceptor conjugated block copolymers, which contain both hole-conductive (p-type) and electron-conductive (n-type) polymer blocks, can be used directly in an OPV, but relatively few examples exist and limited information on the microstructure of these materials is available. Recent work has demonstrated improved performance and nanoscale self-assembly in donor–acceptor conjugated block copolymers,[14,15] and crystalline nanofibers and microphase segregation have been observed in conjugated block copolymer systems.[15−25] However, more versatile synthetic methods are needed to access block copolymers with targeted block lengths and desired optoelectronic properties.

Conjugated block copolymers have been synthesized via a macroreagent approach that utilizes two distinct polymerization reactions[16,26−29] or through sequential monomer addition using a controlled polymerization reaction, such as Grignard metathesis (GRIM)[24,30−32] or catalyst-transfer Suzuki–Miyaura polymerization.[33,34] While these latter approaches have several practical advantages, the macroreagent approach has been more popular for the synthesis of donor–acceptor conjugated block copolymers[14,17,28] since the preparation of donor and acceptor conjugated block copolymers typically requires distinct polymerization reactions. However, the macroreagent approach typically gives poor control over the sizes of each polymer block. Previous work by us[16,35] and others[14,36] has relied on a

Received: December 21, 2012
Revised: March 15, 2013
Published: March 26, 2013

 © 2013 American Chemical Society

Suzuki–Miyaura or Stille polycondensation reaction, which are uncontrolled polymerization reactions and give final products with block lengths dependent on polymer solubility and reaction conditions. Furthermore, the macroreagent approach typically yields block copolymers with significant homopolymer impurities, requiring tedious purification methods to isolate pure block copolymer.[16,36]

An alternative route to conjugated block copolymers is to couple two conjugated polymers, which have been independently synthesized, by an efficient chemical reaction. This gives better control over block lengths since each block is synthesized, purified, and characterized prior to coupling. Click coupling reactions, in particular copper(I)-catalyzed cycloadditions, have been successfully applied as postpolymerization coupling reactions to make rod–coil block copolymers[37−41] and block copolythiophenes[42] but not for the preparation of donor–acceptor conjugated block copolymers. This synthetic route provides block copolymers with a nonconjugated linker, whereas most previous work has primarily focused on materials with continuous conjugation between the blocks. One example of conjugated donor/acceptor polymer joined by a nonconjugated linker has been reported. The sample showed cocrystallization of the constituent blocks and improved photovoltaic performance relative to blends of the corresponding homopolymers.[43,44]

Herein, we demonstrate a click coupling approach for the synthesis of poly(3-hexylthiophene)-*block*-poly(9,9-dioctylfluorene) (P3HT-*b*-PF) conjugated block copolymers. This method is used to prepare a series of P3HT-*b*-PF block copolymers with varying composition. The resulting block copolymers consist of two conjugated polymers linked by a nonconjugated segment. The microstructure of the block copolymers is characterized using a combination of differential scanning calorimetry (DSC) and grazing incidence wide/small-angle X-ray scattering (GIWAXS/GISAXS) to establish qualitative relationships between block lengths and phase behavior of the materials. We find that crystallization of one block is predominant in the film microstructure for all block copolymers studied, but near 50% weight ratios, crystallization of both blocks is achieved. Since the electronic properties of conjugated polymers are known to be correlated with crystallinity, these results suggest that conjugated block copolymers with balanced block ratios may be optimal for use in polymer OPVs.

RESULTS AND DISCUSSION

Synthesis of Conjugated Diblock Copolymers via Click Chemistry. The approach used to prepare conjugated block copolymers involves copper(I)-catalyzed alkyne–azide click coupling of two conjugated polymers. P3HT and PF were chosen for this study, but the general synthetic procedure can be applied to a wide range of polymers made by GRIM and Suzuki–Miyaura polycondensation. Alkyne end-functionalized P3HT with a targeted molecular weight and relatively low polydispersity (PDI) was synthesized via GRIM using previously reported procedures (Table 1, P3HT1 and P3HT2).[45] As discussed in a recent publication, these materials were found to be unstable in oxygen and were used immediately or stored under vacuum in the dark to prevent degradation.[46]

The preparation of a series of PF polymers of varying molecular weight and controlled end-functionality is a more significant challenge. Previous studies on block copolymers that incorporate a PF block have primarily focused on short (3 kg/mol) PF blocks synthesized using $Pd[PPh_3]_4$ catalyst.[47,48] In more recent work, Yokozawa et al. reported a chain-growth polymerization reaction for the synthesis of PF using a modified Pd catalyst with a t-Bu_3P ligand.[49] This is a more active catalyst and enables the room-temperature polycondensation of poly(dialkyl fluorenes) and other monomers. Here, we use modifications of these prior strategies to prepare a series of hydroxyl-functionalized PFs (PF-OH). In the first approach (Scheme 1a), PF-OH was synthesized via Suzuki–Miyaura polycondensation in toluene using $Pd[PPh_3]_4$ catalyst and 4-bromobenzyl alcohol as an end-capper. As shown in Table 1, PF-OH produced using this method (PF1) has a broad molecular weight distribution, as expected for Suzuki–Miyaura polycondensation reaction. ^{1}H NMR analysis shows the final product is end-functionalized (Figure 1), and as discussed below, the end group can be modified for click coupling to P3HT-alkyne.

Table 1. P3HT and PF Homopolymer Samples Prepared

			SEC-MALLS analysis			^{1}H NMR analysis
	name	synthesis method	M_w (kg/mol)	M_n (kg/mol)	PDI	mass per end group (kg/mol)
1	PF1	Suzuki–Miyaura-$Pd[PPh_3]_4$	8.2	5.3	1.55	33.0
2	PF2	Suzuki–Miyaura-$Pd[t\text{-}Bu_3P]_2$	7.4	3.6	2.05	3.9
3	PF3	Suzuki–Miyaura-$Pd[t\text{-}Bu_3P]_2$	11.0	5.5	2.03	7.8
4	PF4	Suzuki–Miyaura-$Pd[t\text{-}Bu_3P]_2$	9.6	4.9	1.99	39.0
5	P3HT1	GRIM	12.0	11.0	1.04	
6	P3HT2	GRIM	6.9	6.1	1.12	

In the second approach, a modified Pd catalyst with protected hydroxyl functionality is prepared and used to initiate Suzuki–Miyaura polycondensation (Scheme 1b). This approach is similar to that reported previously by Yokozawa et al.[49] with a silane-protected hydroxyl functionality incorporated into the catalyst. The catalyst is synthesized in a one-step reaction with $Pd[t\text{-}Bu_3P]_2$. Because of the more active t-Bu_3P ligand, the Suzuki–Miyaura polymerization can be carried out at room temperature in the presence of a mild base. After polymerization, the silane-protecting group is removed by addition of n-tetrabutylammonium fluoride (TBAF) to yield PF-OH. As indicated in Table 1, the PF samples produced using this approach (PF2, PF3, and PF4) are not well-controlled with respect to polydispersity. The broad molecular weight distribution suggests that the bulky silane-protecting group or the presence of excess end-capper may interfere with the catalyst-transfer mechanism reported previously for a similar catalyst.[49] For all PF polymers produced using this method, ^{1}H NMR indicates the presence of a hydroxyl end group.

The degree of end-functionality can be assessed by comparing the molecular weight obtained from ^{1}H NMR with SEC-MALLS analysis, which provides an absolute molecular weight. For PF2 and PF3, ^{1}H NMR and SEC-MALLS indicate a high degree of functionalization since the molar content of polymer end groups estimated by ^{1}H NMR is

dx.doi.org/10.1021/ma3026223 | Macromolecules 2013, 46, 2636−2645

Scheme 1. Preparation of PF-OH and PF-N_3: (a) Preparation of PF-OH via Pd[PPh_3]$_4$-Catalyzed Suzuki–Miyaura polymerization;[a] (b) Preparation of PF-OH via Suzuki–Miyaura Using Modified Pd Catalyst with *t*-Bu_3P Ligand; (c) Preparation of PF-N_3 by Coupling PF-OH with Azidoacetic Acid

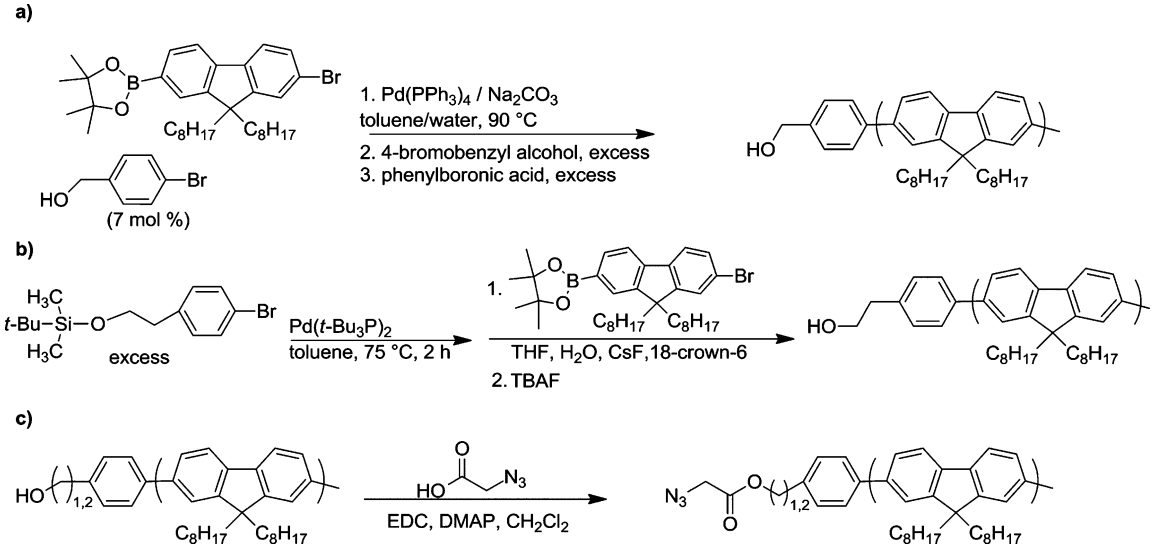

[a]4-Bromobenzyl alcohol is added at the start of the reaction (7 mol %) and then after polymerization in excess to quench the reaction.

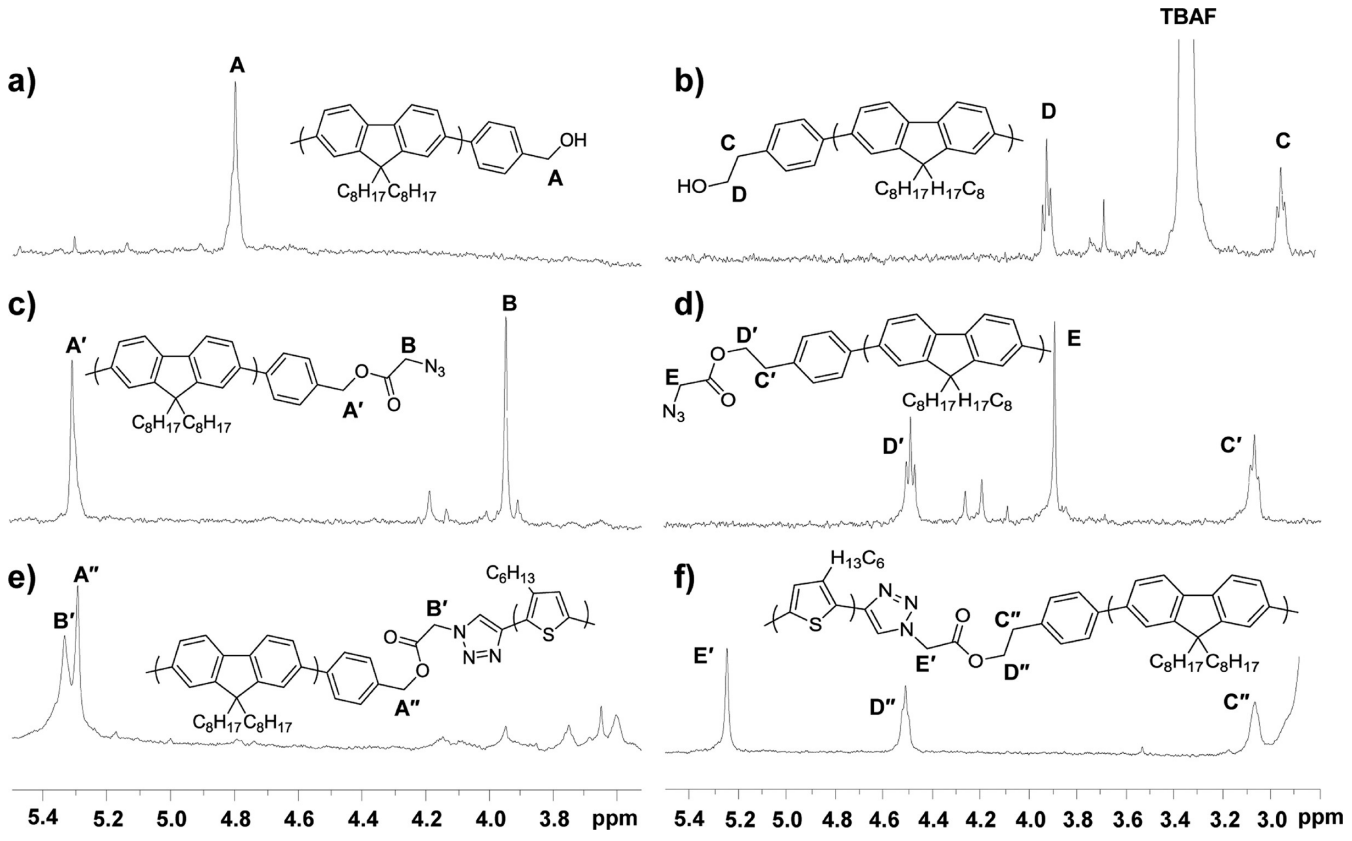

Figure 1. ^{1}H NMR spectra for polymeric intermediates and block copolymers. (a) PF-OH (PF1) produced via Pd[PPh_3]$_4$-catalyzed Suzuki–Miyaura polycondensation. (b) PF-OH (PF2–4) produced via Suzuki–Miyaura polymerization using modified Pd catalyst with *t*-Bu_3P ligand. (c, d) PF-N_3 resulting from coupling of PF-OH with azido acetic acid. (e, f) P3HT-*b*-PF conjugated block copolymers resulting from click coupling of PF-N_3 with alkyne-terminated P3HT.

in good agreement with SEC-MALLS analysis. For PF1 and PF4, the large molecular weight estimate from NMR indicates that a significant amount of unfunctionalized PF is present, and this was also confirmed by MALDI-TOF MS analysis (see Supporting Information Figures S1 and S2). Thus, the modified synthetic methods used for the preparation of PF-OH yield a mixture of functionalized and unfunctionalized polymer for PF1 and PF4.

With these limitations in mind, all four PF samples were used in the preparation of conjugated block copolymers. All PF

dx.doi.org/10.1021/ma3026223 | *Macromolecules* 2013, 46, 2636–2645

Scheme 2. Preparation of P3HT-*b*-PF via Copper-Catalyzed Azide−Alkyne Click Chemistry

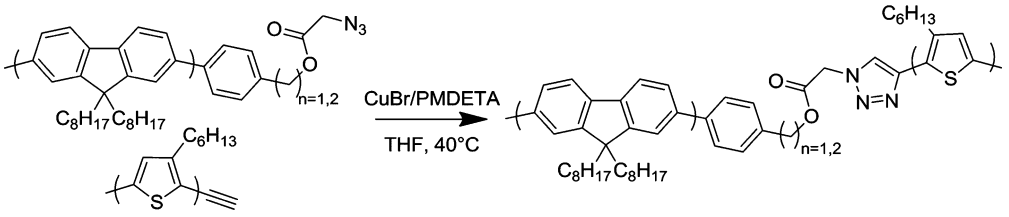

polymers contain end groups which can be derivatized for click coupling. As shown in Scheme 1c, PF-N_3 is prepared by coupling PF-OH with azido acetic acid. ^{1}H NMR reveals a shift of the terminal α-hydroxy protons, indicating complete conversion of the hydroxyl end group to an azide end group (Figure 1c,d). Next, click coupling of P3HT-alkyne and PF-N_3 (Scheme 2) was carried out in THF in the presence of Cu(I)Br and PMDETA. An excess of the PF macroreagent (20 mol % based on ^{1}H NMR ratio of repeat unit to end group) was added to ensure full reaction of the P3HT-alkyne and to compensate for any errors in estimates of functionalization. After the reaction was complete, typically less than 8 h or overnight, the product was run through an alumina column, precipitated in hexanes, and washed with boiling hexanes to remove unreacted PF. This was carried out with five different combinations of P3HT-alkyne and PF-N_3 to yield a series of P3HT-*b*-PF block copolymers (Table 2).

Table 2. P3HT-*b*-PF Conjugated Block Copolymer Samples

sample	source polymers	mass % P3HT by ^{1}H NMR	M_w by SEC-MALLS (kg/mol)	PDI
P3HT79-*b*-PF21	PF2, P3HT1	79	19.0	1.22
P3HT64-*b*-PF36	PF1, P3HT1	64	17.0	1.27
P3HT52-*b*-PF48	PF3, P3HT2	52	17.0	1.53
P3HT32-*b*-PF68	PF1, P3HT2	32	18.0	1.38
P3HT23-*b*-PF77	PF4, P3HT2	23	19.0	1.50

The composition, purity, and molecular weight distributions of the final block copolymer products can be determined by ^{1}H NMR and SEC with both MALLS and UV/vis detection. In all cases, SEC-RI revealed a shift in the molecular weight distribution of the polymeric product relative to the starting macroreagents (see Figure 2a and Supporting Information Figure S3). SEC with UV/vis detection can be used to detect homopolymer impurities and measure the molecular weight distribution for each polymer block separately (see Methods for details of this analysis). A representative example of SEC-UV/vis analysis is shown for P3HT64-*b*-PF36 in Figure 2b,c, and a good match in the molecular weight distributions and at two distinct wavelengths indicates pure block copolymer product with little or no residual homopolymer. A similar shift in the UV/vis trace at 450 nm was observed for P3HT79-*b*-PF21 and P3HT52-*b*-PF48, which indicates complete reaction of the P3HT macroreagent. As expected, block copolymers resulting from the coupling of PF2 and PF3 gave results consistent with the molecular weights of the corresponding homopolymers.

In the case of block copolymers resulting from the coupling of PF1 and PF4, the measured molecular weight of the final block copolymers is inconsistent with the constituent homopolymers. This may due to the presence of homopolymer impurities caused by unfunctionalized PF chains in PF1 and PF4. High molecular weight homopolymer impurities might

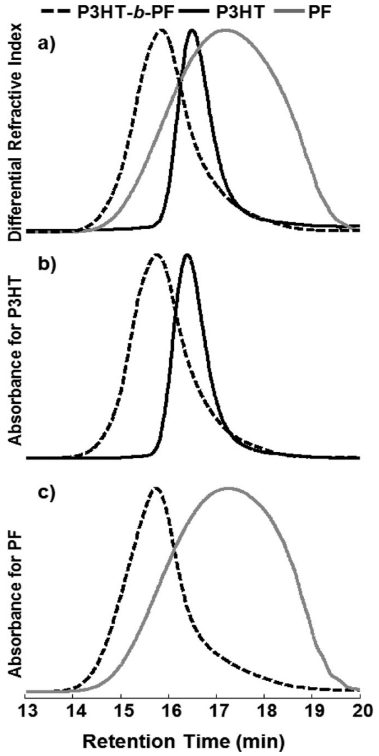

Figure 2. SEC analysis of P3HT64-*b*-PF36 and corresponding P3HT and PF macroreagents. (a) SEC-RI analysis showing a shift in the molecular weight distribution of the final block copolymer relative to the P3HT and PF macroreagents. (b) SEC-UV/vis analysis at 450 nm showing a shift in the molecular weight distribution of the P3HT block relative to the starting P3HT macroreagent. (c) SEC-UV/vis analysis at 300 nm (corrected for the absorbance of the P3HT block) showing a shift in the molecular weight distribution of the PF block relative to starting PF1 macroreagent.

remain after solvent washing. Additionally, extensive solvent washing may bias the distribution by removing lower molecular weight block copolymer. Thus, obtaining precursor materials that have a high degree of functionality remains a significant obstacle to obtain well-defined materials via this route. However, in all cases, a clear shift is observed in the SEC-RI and corrected 300 nm UV/vis traces, indicating the formation of block copolymer product. SEC analysis shows that block copolymer is the major product resulting from coupling, and ^{1}H NMR analysis shows the P3HT content in the block copolymer series varies from 23 up to 79 wt %. As a result, while residual homopolymer impurities were present in some samples, this synthetic method enables the preparation of a series of conjugated block copolymers with systematic variation of the block ratios.

Crystallization of Conjugated Block Copolymers. Both crystallization and chain orientation impact charge transport in

dx.doi.org/10.1021/ma3026223 | *Macromolecules* 2013, 46, 2636−2645

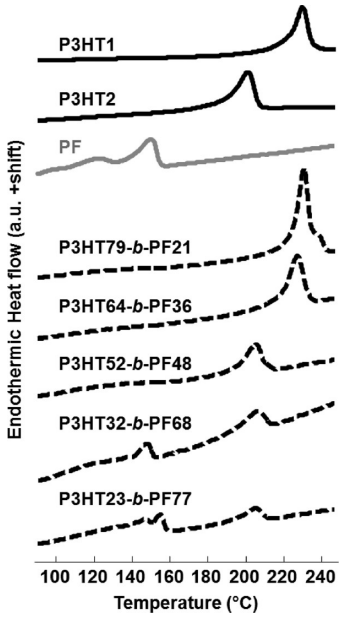

Figure 3. Differential scanning calorimetry (DSC) analysis for P3HT1, P3HT2, PF3, and P3HT-*b*-PF block copolymers. All PF homopolymers studied here show a crystallization transition near 150 °C.

conjugated polymer thin films. In the case of P3HT, larger charge mobilities are correlated with increased crystallinity due to improved $\pi-\pi$ stacking,[50] and the highest charge mobilities are measured in the direction parallel to the $\pi-\pi$ stacking direction and along the polymer backbone.[51,52] However, several polymers with exceptional performance in bulk heterojunction OPVs have been found to have a low degree of crystallinity.[53] In some cases, thermal annealing decreases the performance of OPV devices, and the optimal performance is thought to depend on phase separation and organization at hierarchical length scales.[53−55] As a result, in conjugated block copolymers, crystallization of one or both blocks may impact performance. The series of conjugated block copolymers prepared in this study enables an investigation into the role of polymer block lengths and composition on crystallization and self-assembly behavior.

DSC measurements (Figure 3) indicate a crystal melting transition near 230 °C for P3HT1, 200 °C for P3HT2, and 150 °C for PF polymers. P3HT-*b*-PF block copolymers show a peak corresponding to P3HT at either 230 or 200 °C, depending on the source polymer used. The temperature of the thermal transition corresponding to P3HT does not change in the block copolymers relative to the source P3HT homopolymers and is present in all P3HT-*b*-PF block copolymers studied. A peak corresponding to PF crystal melting is only present in block copolymers with PF as the majority block but not for block copolymers with majority P3HT. Thus, the crystallization of PF is suppressed in P3HT-*b*-PF when the P3HT weight fraction is greater than 52%.

GIWAXS analysis was carried out to examine the characteristics and orientation of crystallites present in the samples. Samples were heated at or above 230 °C to melt any crystals present and then subsequently cooled to 100 °C for measurement. Samples subjected to 5 days of 1,2-dichlorobenzene solvent annealing were also investigated but did not show as strong crystallization as the thermally annealed samples. As shown in Figure 4, crystallites were found for all samples, with qualitatively different diffraction patterns observed with changing block ratios. These diffraction patterns correspond to those of either pure P3HT or PF, as shown in Figures S4 and S5. For block copolymers that contain majority P3HT (P3HT79-*b*-PF21, P3HT64-*b*-PF36, P3HT52-*b*-PF48), P3HT crystallites dominate the morphology. GIWAXS reveals characteristic (100), (200), and (300) peaks oriented along the q_z-axis, normal to the substrate. These peaks correspond to spacing between the backbones through the alkyl side chains, and the GIWAXS scattering pattern indicates an in-plane $\pi-\pi$ stacking direction, typical of regioregular P3HT.[51,52] PF crystallization is suppressed for P3HT79-*b*-PF21 and P3HT64-*b*-PF36, but some evidence of weak PF crystallinity can be seen for P3HT52-*b*-PF48. Conversely, for block copolymers with a majority PF block, P3HT32-*b*-PF68 and P3HT23-*b*-PF77, PF crystallinity is predominant. The pattern observed corresponds to the α-phase of PF previously seen in oriented PF fibers.[56,57]

Some evidence for P3HT crystallinity is apparent in P3HT32-*b*-PF68, but exclusively PF crystallites are detected in P3HT23-*b*-PF77. Line cuts of the GIWAXS data, provided in Figure S5, confirm this observation. This indicates that thin film confinement may play a role in suppressing some P3HT crystallization, reflected by DSC measurements of all bulk samples (Figure 3).

These results indicate that competitive crystallization occurs in P3HT-*b*-PF. While some indication of crystallization of both blocks is seen in block copolymers with roughly balanced block

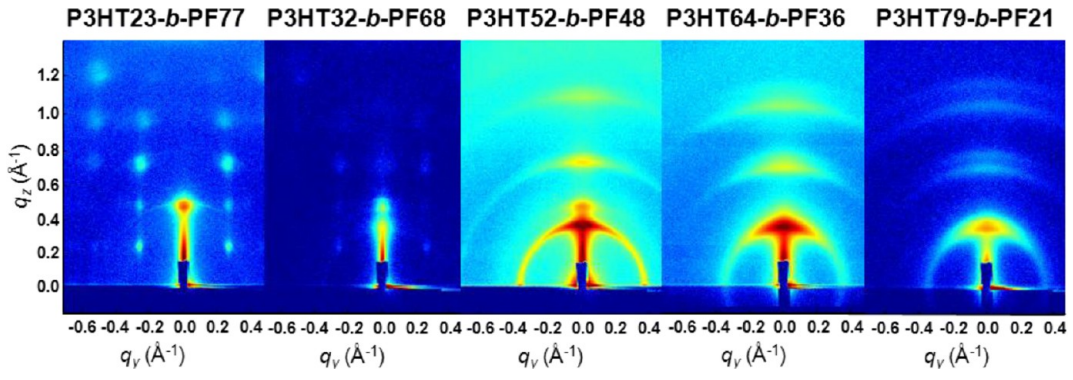

Figure 4. GIWAXS patterns for P3HT-*b*-PF block copolymer films thermally annealed at 230 °C and measured at 100 °C at an incidence angle of 0.25°. Materials with high PF content show crystallinity characteristic of highly ordered PF crystallites while block copolymers with a high P3HT content show exclusively P3HT crystallites. P3HT52-*b*-PF48 and P3HT32-*b*-PF68 films show evidence for both P3HT and PF crystals.

dx.doi.org/10.1021/ma3026223 | *Macromolecules* 2013, 46, 2636−2645

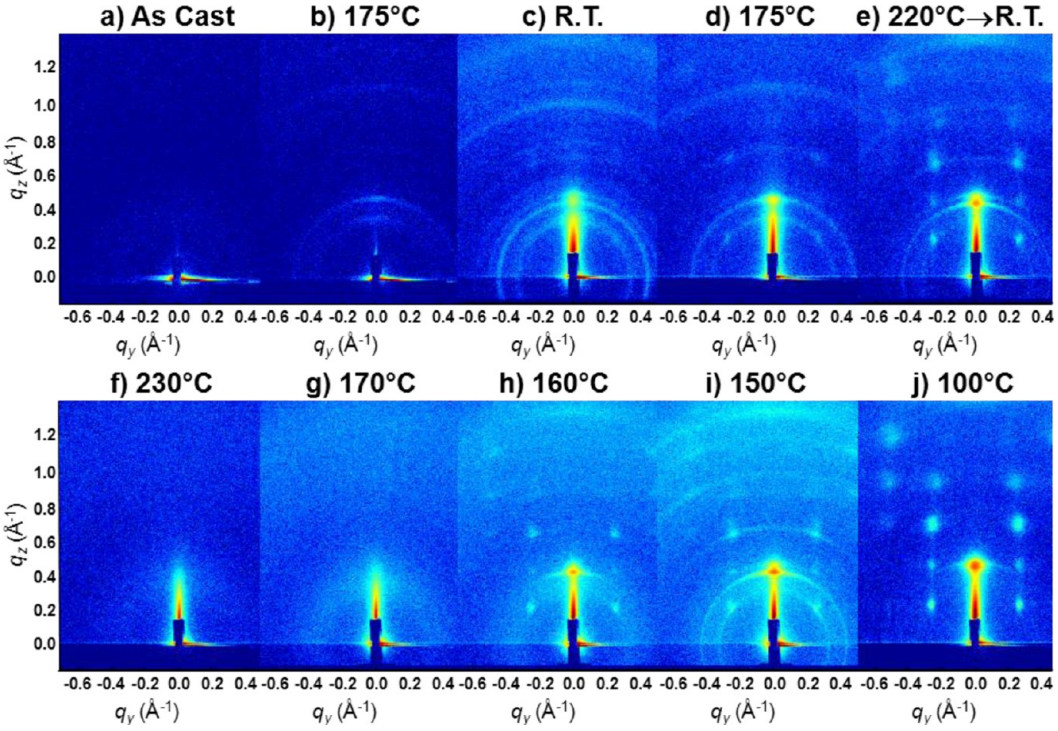

Figure 5. Temperature-dependent GIWAXS analysis of P3HT23-*b*-PF77 film at an incidence angle of 0.25°. The film was measured sequentially from left to right: (a) as-cast, (b) heat to 175 °C, and (c) return to room temperature. Then (d) heat to 175 °C, (e) continue heating to 220 °C and hold for several hours before returning to room temperature, (f) heat to 230 °C allowing all crystal features to melt, and slowly cool to (g) 170, (h) 160, (i) 150, and (j) 100 °C.

weight fractions, most samples indicate the predominance of one type of crystallite. Transmission electron microscopy and X-ray diffraction studies of the α-phase of PF indicate that chains are not organized in a face-to-face packing structure,[8,56] in contrast to the structure of P3HT crystallites. This mismatch between crystal structures and confinement in a thin film may explain the predominance of one type of crystallite in the samples studied. These results are consistent with previous studies of double-crystalline diblock copolymers which found that the crystallization behavior could be broadly tuned by changing the composition of the block copolymer, and in some cases, competitive crystallization occurs.[58−61] These results are also consistent with previous work from our group on P3HT conjugated block copolymers with conjugation across the linker.[16,35] In general, the majority block is observed to dominate crystallization or suppress crystallization of the second block.[35] In the case of P3HT-*b*-PF reported here, similar behavior is observed, and crystallization of both blocks is only possible when the block weight fractions are in balance, with P3HT wt % ranging between 32 and 52. This suggests that the flexible linker has a relatively small impact on film morphology and polymer crystallization. Also, on the basis of the good match in the peak positions for P3HT-*b*-PF and pristine P3HT and PF homopolymer films, we infer that crystalline domains in the block copolymer films consist of pure P3HT or PF polymer blocks, which suggests that phase separation between the polymer blocks occurs during crystallization.

Extensive temperature-dependent measurements were performed on P3HT23-*b*-PF77, which has a majority PF block (Figure 5). The as-cast sample is largely featureless, but upon heating to 175 °C, above the crystallization temperature of PF but below that of P3HT, and cooling back to room temperature, only faint crystal peaks emerge. The sample was subsequently heated to 220 °C, above the crystallization temperature for both constituent polymer blocks, before cooling down to room temperature, resulting in ordered PF crystallite peaks. The sample was then heated to 230 °C to completely melt any P3HT crystals and slowly cooled while measuring at 170, 160, 150, and 100 °C. While the final GIWAXS pattern appears to indicate only PF crystallites are present, heating the film above the crystallization temperature of P3HT is necessary to achieve well-oriented PF crystallite peaks. This suggests that, consistent with DSC measurements, some P3HT crystallites may be present in as-cast films and play a role in the PF crystallization kinetics in thin films.

No clear evidence for microphase segregation was observed by GISAXS (see Figure S6). Samples subjected to thermal annealing and solvent annealing in the presence of 1,2-dichlorobenzene at room temperature and 150 °C failed to give any indication of an ordered nanostructure. The lack of a self-assembled mesophase may be due to the high crystallization temperatures of the polymers or the specific processing conditions chosen.

Crystallization of both blocks in double crystalline block copolymers has been previously reported for a range of nonconjugated block copolymers in both the strong[62] and weak segregation regimes as well as for block copolythiophenes.[15,19,22−24,31,32] P3HT-based block copolymers with one nonconjugated block typically exhibit a crystalline, nanowire morphology characteristic of P3HT crystallites,[41,46,63−66] and previous work with donor/acceptor conjugated block copolymers has typically found exclusive crystallization of the P3HT block.[14,16] The results reported here demonstrate that crystallization of both blocks in conjugated block copolymers can be achieved by proper

dx.doi.org/10.1021/ma3026223 | *Macromolecules* 2013, 46, 2636−2645

balance of the molecular weight ratios. This may be important for achieving optimal active layer morphology and favorable electronic properties in all-polymer OPVs and other organic electronic devices. Crystallization of P3HT is correlated with high charge carrier mobilities and improved performance in a photovoltaic device, and depending on the second polymer block chosen, crystallization of the second polymer block may be less important.[53−55] This work also highlights the challenges in achieving a self-organized structure in conjugated block copolymers. High crystallization temperatures and long relaxation times may require modification of conventional annealing procedures to achieve microphase segregation. Future work will focus on tailoring the properties of conjugated block copolymer films and on the development of new annealing procedures for achieving self-organization.

CONCLUSION

Herein, we have demonstrated a new route for synthesis of conjugated block copolymers using click chemistry. The principal advantage of this synthetic route is the ability to characterize and/or purify the starting materials fully before the coupling reaction, and a single starting polymer may be coupled with multiple different products to give a variety of materials. Obtaining precursor materials that have a high degree of chain-end functionality remains a significant obstacle to obtaining well-defined materials by this route. While we are able to obtain reasonably well-defined materials by removing the highly soluble PF impurities, not all block copolymer systems will be able to take advantage of differential solubility. We find that in P3HT-*b*-PF crystallization of the majority block is predominant at extreme block ratios, and at intermediate ratios crystallization of both blocks occurs. The resulting crystallites are highly aligned with an in-plane $\pi-\pi$ stacking direction for P3HT crystallites and the observation of a PF α-phase for PF crystallites. Microphase segregation was not observed in any of the thermally annealed samples. The thin film structure observed is similar to that of conjugated block copolymers with conjugation across the linker, indicating that the presence of a flexible linker does not have a significant impact on film morphology or polymer crystallization.

METHODS

Instrumentation. *Nuclear Magnetic Resonance Spectroscopy (NMR).* Solution ^{1}H NMR spectroscopy was performed on a 500 MHz Varian Inova NMR spectrometer and a Bruker 400 MHz multinuclear spectrometer. Chloroform-*d* ($CDCl_3$, Cambridge Isotope Laboratories) was used as the solvent with TMS (0.05%) as an internal standard. Data were processed using SpinWorks 3.1.8.1.[67]

Size-Exclusion Chromatography (SEC). Polymer molecular weights and polydispersities (PDIs) were obtained by SEC using an Agilent 1200 module equipped with three PSS SDV columns in series (100, 1000, and 10 000 Å pore sizes), an Agilent variable wavelength UV/vis detector, a Wyatt Technology HELEOS II multiangle laser light scattering (MALLS) detector (λ = 658 nm), and a Wyatt Technology Optilab reX RI detector. This system enables SEC with simultaneous refractive index (SEC-RI), UV/vis (SEC-UV/vis), and MALLS (SEC-MALLS) detection. THF was used as the mobile phase at a flow rate of 1 mL/min at 40 °C. Weight-average molecular weights (M_w) are determined by light scattering with d*n*/d*c* values calculated using assuming 100% mass recovery of the injected sample. Polydispersity (PDI) was determined using SEC-RI calibrated with a set of monodisperse polystyrene standards (Astra Software Version 5.3.4).

The molecular weight distributions for each polymer block and corresponding homopolymer impurities can be obtained by SEC-UV/vis analysis at two distinct wavelengths. First, by using a wavelength specific to one polymer block, we can obtain the molecular weight distribution for one block only. In the case of P3HT-*b*-PF, 450 nm is specific to P3HT since PF has negligible absorbance at this wavelength. Next, SEC-UV/vis analysis at a second wavelength sensitive to both polymer blocks can be corrected to obtain the molecular weight distribution of the second block. In the case of P3HT-*b*-PF, analysis at 300 nm is sensitive to both blocks, but the contribution of P3HT to the signal is subtracted using the 450 nm SEC-UV/vis trace and the absorbance ratio for P3HT at 450 nm relative to 300 nm, measured independently to be 5.4. The 300 nm absorbance trace presented in Figure 2 and Figure S3 is the result of this subtraction and reflects the molecular weight distribution of the PF blocks only.

MALDI-TOF MS. MALDI-TOF MS spectra were collected using a Bruker Daltonics Autoflex II mass spectrometer, which is equipped with an N_2 laser, (λ = 337 nm) operating at a frequency of 25 Hz and an accelerating voltage of 20 kV. *trans*-2-[3-(4-*tert*-Butylphenyl)-2-methyl-2-propenylidene]malononitrile (DCTB) (>98%, TCI) was used as the matrix. Solutions of DCTB (20 mg/mL) and the analyte (10 mg/mL) were prepared in THF and then mixed in a 10:2 ratio. A volume of 1 μL was applied to the target via the dried droplet method.[68] Mass spectra were collected in reflectron mode, and the instrument was externally calibrated with polystyrene standards.

Differential Scanning Calorimetry (DSC). Thermograms were recorded on a TA Instruments DSC 2920 equipped with a refrigerated cooling system against an empty sealed pan as reference. In a typical run, the sample was heated to 250 °C at 5 °C/min, cooled to 40 °C at 5 °C/min, and then equilibrated for 10 min before heating to 250 °C at 5 °C/min. Second heating cycles are reported.

Grazing Incidence Small/Wide-Angle X-ray Scattering (GISAXS/GIWAXS). Grazing incidence small/wide-angle X-ray scattering measurements were carried out on Sector 8 at the Advanced Photon Source, Argonne National Laboratory.[69] Beamline 8-ID-E operates at an energy of 7.35 keV, and images were collected from a Pilatus 1MF camera (Dectris), with two exposures for different vertical position of the detector. After flat-field correction for detector nonuniformity, the images are combined to fill in the gaps for rows at the borders between modules, leaving dark only the columns of inactive pixels at the center. Using the GIXSGUI package for MATLAB (MathWorks), data are corrected for X-ray polarization, detector sensitivity, and geometrical solid angle.[70] For GIWAXS, the beam size is 200 μm (h) × 20 μm (v), and the sample−detector distance is 204 mm. For GISAXS, the beam size is 100 μm (h) × 50 μm (v), and the sample−detector distance is 2185 mm. Sample measurement and thermal annealing were carried out under vacuum, with the sample stage interfaced with a Lake Shore 340 unit.

Materials. Anhydrous tetrahydrofuran (THF), 1,3-bis(diphenylphosphino)propane]dichloronickel(II) (Ni[dppp]Cl_2), isopropylmagnesium chloride (^{i}PrMgCl) 2 M in THF, ethynylmagnesium bromide 0.5 M in THF, 9,9-dioctyl-2,7-dibromofluorene, 9,9-dioctylfluorene-2,7-diboronic acid bis(1,3-propanediol) ester, 4-bromobenzyl alchohol, phenylboronic acid, magnesium sulfate ($MgSO_4$), copper(I) bromide (CuBr), 18-crown-6, cesium fluoride (CsF), *N*,*N*,*N*′,*N*″,*N*″-pentamethyldiethylenetriamine (PMDETA), 4-bromophenethyl alcohol, imidazole, tetrakis(triphenylphosphine)-palladium(0) ($Pd[PPh_3]_4$), bis(tri-*tert*-butylphosphine)palladium(0) ($Pd[t\text{-}Bu_3P]_2$), 1-ethyl-3-(3-(dimethylamino)propyl)carbodiimide (EDC), 4-(dimethylamino)pyridine (DMAP), 1.0 M tetrabutylammonium fluoride solution in THF (TBA), and sodium azide were obtained from Aldrich and used as received. 2,5-Dibromo-3-hexylthiophene, 7′-bromo-9′,9′-dioctylfluoren-2′-yl-4,4,5,5,-tetramethyl[1,3,2]dioxaborolane, and azido acetic acid were synthesized as previously described.[71−73] Alkyne-terminated P3HT was synthesized by a method described elsewhere.[46]

Hydroxyl-Functionalized Poly(9,9-dioctylfluorene) (PF-OH) via $Pd[PPh_3]_4$-Catalyzed Suzuki−Miyaura Polycondensation. In a typical procedure, 2.1 g (3.6 mmol) of 7′-bromo-9′,9′-dioctylfluoren-2-yl-4,4,5,5-tetramethyl[1,3,2]dioxaborolane, 46 mg (0.25 mmol) of 4-bromobenzyl alcohol, and 50 mg (43 μmol) of $Pd[PPh_3]_4$ were added to a Schlenk tube and degassed under vacuum followed by backfilling

with nitrogen. A mixture of purged toluene (10 mL), water (10 mL), and Aliquot 336 (a few drops) was then added by cannula. The vessel was reacted for 22 h at 90 °C, after which 0.25 g (1.3 mmol) of 4-bromobenzyl alcohol was added to quench the reaction. The reaction was allowed to proceed an additional 20 h followed by addition of 0.27 g (2.2 mmol) of phenylboronic acid. The polymer was precipitated into methanol and washed with acetone overnight in a Soxhlet extractor followed by collection in dichloromethane to give product **1**. Yield: 1.4 g. ^{1}H NMR ($CDCl_3$, ppm): δ = 7.84 (d, 2*n*H, Ar−*H*), 7.71 (d, 2*n*H, Ar−*H*), 7.68 (s, 2*n*H, Ar−*H*), 2.13 (m, 4*n*H, Ar−C−CH_2−), 1.30−1.00 (m, 20*n*H, −CH_2−), 0.85 (m, 4*n*H, −CH_2−), 0.82 (t, 6*n*H, −CH_3), 4.79 (s, 2H, Ar−CH_2−OH).

1-Bromo-4-[2-[[(1,1-dimethylethyl)dimethylsilyl]oxy]ethyl]-benzene. 4-Bromophenethyl alcohol (2.5 g, 12.6 mmol) was dissolved in 6 mL of dry DMF in a 25 mL round-bottom flask. The solution was purged with N_2 before adding *tert*-butyldimethylsilane (2.47 g, 16.4 mmol). Imidazole (2.24g, 32.8 mmol) was dissolved in 10 mL of DMF in a separate flask. Both flasks were cooled to 0 °C in an ice bath before transferring the imidazole solution to the reaction flask by cannula. The reaction solution was stirred at rt for 4 h before quenching by the addition of water and hexanes, collecting the organic layer, and drying over $MgSO_4$. The final product was purified by column chromatography (5% ethyl acetate/hexanes) to collect 1.91 g (48% yield) of a clear oil. ^{1}H NMR ($CDCl_3$, ppm): δ = 7.39 (d, 2H, Ar−*H*), 7.08 (d, 2H, Ar−*H*), 3.78 (t, 2H, Ar−CH_2−CH_2−O−Si), 2.76 (t, 2H, Ar−CH_2−CH_2−O−Si), 0.86 (s, 9H, Si−C−CH_3), −0.02 (s, 6H, Si−CH_3).

***t*-Bu$_3$PPd[PhCH$_2$CH$_2$OSi(CH$_3$)$_2$C(CH$_3$)$_3$]Br.** In a typical procedure, Pd[*t*-Bu_3P]$_2$ (21.5 mg, 0.042 mmol) was dissolved in 0.2 mL of toluene in an inert atmosphere glovebox, and an excess of 1-bromo-4-[2-[[(1,1-dimethylethyl)dimethylsilyl]oxy]ethyl]benzene (170 mg, 0.539 mmol) was added. The solution was stirred at 75 °C for 2 h and then allowed to cool to room temperature. The crude product was used without purification.

Hydroxyl-Functionalized Poly(9,9-dioctylfluorene) (PF-OH) via *t*-Bu$_3$PPd[PhCH$_2$CH$_2$OSi(CH$_3$)$_2$C(CH$_3$)$_3$]Br-Catalyzed Suzuki−Miyaura Polymerization. 7′-Bromo-9′,9′-dioctylfluoren-2-yl-4,4,5,5-tetramethyl[1,3,2]dioxaborolane (0.51 g, 0.86 mmol) was dissolved in 30 mL of THF along with 18-crown-6 (1.56 g, 5.9 mmol), CsF (0.4.0 g, 3.1 mmol), and 1.5 mL of DI water. The monomer solution was purged with N_2 for 30 min before adding the crude product solution from the preparation of *t*-Bu_3PPd [$PhCH_2CH_2OSi(CH_3)_2C(CH_3)_3$]-Br. The solution was stirred overnight at room temperature before quenching with 1 mL of 5 M HCl. The polymer was recovered by precipitation in methanol and washed with copious amounts of acetone. To remove the silane protecting group, the solid product was redissolved in THF (15 mL) at room temperature, and 0.2 mL of TBAF was added. The solution was stirred overnight before recovering the polymeric product by precipitation in methanol to collect a light green solid. Yield: 194 mg, 52% (**2**). ^{1}H NMR ($CDCl_3$, ppm): δ = 7.84 (d, 2*n*H, Ar−*H*), 7.71 (d, 2*n*H, Ar−*H*), 7.68 (s, 2*n*H, Ar−*H*), 2.13 (m, 4*n*H, Ar−C−CH_2−), 1.30−1.00 (m, 20*n*H, −CH_2−), 0.85 (m, 4*n*H, −CH_2−), 0.82 (t, 6*n*H, −CH_3), 3.92 (t, 2H, Ar−CH_2−CH_2−OH), 2.95 (t, 2H, Ar−CH_2−CH_2−OH).

Azide-Functionalized PF (PF-N$_3$). In a typical procedure, 1.4 g (0.14 mmol) of PF-OH was dissolved in dichloromethane at room temperature, and 107 mg of EDC (0.54 mmol) and 21 mg (0.17 mmol) of DMAP were added followed by 136 mg of azidoacetic acid (1.3 mmol). The reaction was allowed to proceed overnight at room temperature, and the resulting solution was then washed with water. The organic phase was collected and the solvent removed in a rotary evaporator. The product was recovered by precipitation in methanol and dried under vacuum.

PF-N$_3$ (PF1). δ = 7.84 (d, 2·*n*H, Ar−*H*), 7.71 (d, 2*n*H, Ar−*H*), 7.68 (s, 2*n*H, Ar−*H*), 2.13 (b, 4*n*H, Ar−C−CH_2−), 1.30−1.00 (m, 20*n*H, −CH_2−), 0.85 (b, 4*n*H, −CH_2−), 0.82 (t, 6*n*H, −CH_3), 5.31 (s, 2H, Ar−CH_2−OOC−), 3.95 (s, 2H, Ar−CH_2−OOC−CH_2−N_3).

PF-N$_3$ (PF2−4). ^{1}H NMR ($CDCl_3$, ppm) δ = 7.84 (d, 2*n*H, Ar−*H*), 7.71 (d, 2*n*H, Ar−*H*), 7.68 (s, 2*n*H, Ar−*H*), 2.13 (m, 4*n*H, Ar−C−CH_2−), 1.30−1.00 (m, 20*n*H, −CH_2−), 0.85 (m, 4*n*H, −CH_2−), 0.82 (t, 6*n*H, −CH_3), 4.48 (t, 2H, Ar−CH_2−CH_2−OOC−), 3.89 (s, 2H, −CH_2−OOC−CH_2−N_3), 3.07 (t, 2H, Ar−CH_2− CH_2−COO).

P3HT-*b*-PF via Copper-Catalyzed Azide−Alkyne Click Coupling. PF-N_3 were reacted with alkyne-terminated P3HT in a click coupling reaction to give P3HT-*b*-PF. In a typical reaction, 0.15 g of P3HT (M_n = 6 kDa, 0.025 mmol) was reacted with an excess of PF (1.2× based on NMR determined functionality) in the presence of CuBr (14 mg, 0.1 mmol) in THF (35 mL) and 0.1 mL of *N*,*N*,*N*′,*N*″,*N*″-pentamethyldiethylenetriamine. P3HT, PF, CuBr, and THF were mixed in air in a 50 mL flask and purged by needle with nitrogen for 30 min before addition of the PMDETA. The reaction was allowed to proceed for at least 8 h at 40 °C. Reaction vessel contents were passed through an alumina column to remove excess copper, and the reaction products were concentrated before precipitation into hexanes. The precipitate was then collected and washed with boiling hexanes to remove excess PF.

P3HT-b-PF (P3HT64-b-PF36 and P3HT32-b-PF68). ^{1}H NMR ($CDCl_3$, ppm) δ = 7.84 (d, 2*n*H, Ar−*H*), 7.71 (d, 2*n*H, Ar−*H*), 7.68 (s, 2*n*H, Ar−*H*), 6.98 (s, 1*m*H, Ar−*H*), 2.80 (t, 2*m*H, Ar−CH_2−), 2.13 (b, 4*n*H, Ar−C−CH_2−), 1.50−1.00 (m, (20*n* + 11*m*)H, −CH_2−), 0.85 (m, 4*n*H, −CH_2−), 0.82 (t, 6*n*H, −CH_3), 5.33 (s, 2H, Ar−CH_2−OOC−), 5.29 (s, 2H,−CH_2−OOC−CH_2−N_3C_2H).

P3HT-b-PF (P3HT79-b-PF21, P3HT52-b-PF48, and P3HT23-b-PF77). ^{1}H NMR ($CDCl_3$, ppm) δ = 7.84 (d, 2*n*H, Ar−*H*), 7.71 (d, 2*n*H, Ar−H), 7.68 (s, 2*n*H, Ar−*H*), 6.98 (s, 1*m*H, Ar−*H*), 2.80 (t, 2*m*H, Ar−CH_2−), 2.13 (b, 4*n*H, Ar−C−CH_2−), 1.50−1.00 (m, 20*n* + 11*m*H, −CH_2−), 0.85 (m, 4*n*H, −CH_2−), 0.82 (t, 6*n*H, −CH_3), 5.25 (s, 2H, −OOC−CH_2−N_3C_2), 4.51 (t, 2H, Ar−CH_2−CH_2−OOC), 3.06 (t, 2H, Ar−CH_2−CH_2−OOC).

■ ASSOCIATED CONTENT

Ⓢ Supporting Information

MALDI-TOF MS spectra, SEC chromatographs, GIWAXS and GISAXS data. This material is available free of charge via the Internet at http://pubs.acs.org.

■ AUTHOR INFORMATION

Corresponding Author

*E-mail rafaelv@rice.edu.

Notes

The authors declare no competing financial interest.

■ ACKNOWLEDGMENTS

The authors acknowledge financial support from the Welch Foundation (Grant #C-1750), the Shell Center for Sustainability, and Louis and Peaches Owen. Authors acknowledge the Mikos group at Rice University for use of their DSC equipment. Use of the Center for Nanoscale Materials and Advanced Photon Source at Argonne National Laboratory was supported by the U.S. Department of Energy, Office of Science, Office of Basic Energy Sciences, under Contract DE-AC02-06CH11357. Authors acknowledge T. Sun, Argonne National Laboratory, for assistance with GIWAXS/GISAXS measurements. Research was carried out in part at the Center for Functional Nanomaterials, Brookhaven National Laboratory, which is supported by the U.S. Department of Energy, Office of Basic Energy Sciences, under Contract DE-AC02-98CH10886. A portion of this research was conducted at the Center for Nanophase Materials Sciences, which is sponsored at Oak Ridge National Laboratory by the Scientific User Facilities Division, Office of Basic Energy Sciences, U.S. Department of Energy.

■ REFERENCES

(1) Zhan, X.; Zhu, D. *Polym. Chem.* **2010**, *1*, 409.

(2) Geffroy, B.; Le Roy, P.; Prat, C. *Polym. Int.* **2006**, *55*, 572−582.
(3) Yu, G.; Pakbaz, K.; Heeger, A. J. *Appl. Phys. Lett.* **1994**, *64*, 3422−3424.
(4) Hoppe, H.; Sariciftci, N. S. *J. Mater. Chem.* **2006**, *16*, 45−61.
(5) Veenstra, S. C.; Loos, J.; Kroon, J. M. *Prog. Photovoltaics* **2007**, *15*, 727−740.
(6) McNeill, C. R.; Greenham, N. C. *Adv. Mater.* **2009**, *21*, 3840−3850.
(7) Yan, H.; Collins, B. A.; Gann, E.; Wang, C.; Ade, H.; McNeill, C. R. *ACS Nano* **2011**, *6*, 677−688.
(8) Zhang, R.; Li, B.; Iovu, M. C.; Jeffries-EL, M.; Sauvé, G.; Cooper, J.; Jia, S.; Tristram-Nagle, S.; Smilgies, D. M.; Lambeth, D. N.; McCullough, R. D.; Kowalewski, T. *J. Am. Chem. Soc.* **2006**, *128*, 3480−3481.
(9) Segalman, R. A.; McCulloch, B.; Kirmayer, S.; Urban, J. J. *Macromolecules* **2009**, *42*, 9205−9216.
(10) Botiz, I.; Darling, S. B. *Mater. Today* **2010**, *13*, 42−51.
(11) Darling, S. B. *Energy Environ. Sci.* **2009**, *2*, 1266.
(12) Scherf, U.; Gutacker, A.; Koenen, N. *Acc. Chem. Res.* **2008**, *41*, 1086−1097.
(13) He, M.; Qiu, F.; Lin, Z. *J. Mater. Chem.* **2011**, *21*, 17039−17048.
(14) Mulherin, R. C.; Jung, S.; Huettner, S.; Johnson, K.; Kohn, P.; Sommer, M.; Allard, S.; Scherf, U.; Greenham, N. C. *Nano Lett.* **2011**, *11*, 4846−4851.
(15) Yu, X.; Yang, H.; Wu, S.; Geng, Y.; Han, Y. *Macromolecules* **2012**, *45*, 266−274.
(16) Verduzco, R.; Botiz, I.; Pickel, D. L.; Kilbey, S. M.; Hong, K.; Dimasi, E.; Darling, S. B. *Macromolecules* **2011**, *44*, 530−539.
(17) Botiz, I.; Schaller, R. D.; Verduzco, R.; Darling, S. B. *J. Phys. Chem. C* **2011**, *115*, 9260−9266.
(18) Yokozawa, T.; Kohno, H.; Ohta, Y.; Yokoyama, A. *Macromolecules* **2010**, *43*, 7095−7100.
(19) Wu, P.-T.; Ren, G.; Kim, F. S.; Li, C.; Mezzenga, R.; Jenekhe, S. A. *J. Polym. Sci., Part A: Polym. Chem.* **2010**, *48*, 614−626.
(20) Kim, F. S.; Ren, G.; Jenekhe, S. A. *Chem. Mater.* **2010**, *23*, 682−732.
(21) He, M.; Zhao, L.; Wang, J.; Han, W.; Yang, Y.; Qiu, F.; Lin, Z. *ACS Nano* **2010**, *4*, 3241−3247.
(22) Ge, J.; He, M.; Qiu, F.; Yang, Y. *Macromolecules* **2010**, *43*, 6422−6428.
(23) Zhang, Y.; Tajima, K.; Hashimoto, K. *Macromolecules* **2009**, *42*, 7008−7015.
(24) Zhang, Y.; Tajima, K.; Hirota, K.; Hashimoto, K. *J. Am. Chem. Soc.* **2008**, *130*, 7812−7813.
(25) Park, J. Y.; Koenen, N.; Forster, M.; Ponnapati, R.; Scherf, U.; Advincula, R. *Macromolecules* **2008**, *41*, 6169−6175.
(26) Woody, K. B.; Leever, B. J.; Durstock, M. F.; Collard, D. M. *Macromolecules* **2011**, *44*, 4690−4698.
(27) Tu, G.; Li, H.; Forster, M.; Heiderhoff, R.; Balk, L. J.; Sigel, R.; Scherf, U. *Small* **2007**, *3*, 1001−1006.
(28) Sun, J.; Zhang, C.; Venkatesan, S.; Li, R.; Sun, S.-S.; Qiao, Q. *J. Polym. Sci. B: Polym. Phys.* **2012**, *50*, 917−922.
(29) Tu, G.; Li, H.; Forster, M.; Heiderhoff, R.; Balk, L. J.; Scherf, U. *Macromolecules* **2006**, *39*, 4327−4331.
(30) Wu, S.; Bu, L.; Huang, L.; Yu, X.; Han, Y.; Geng, Y.; Wang, F. *Polymer* **2009**, *50*, 6245−6251.
(31) Wu, P.-T.; Ren, G.; Li, C.; Mezzenga, R.; Jenekhe, S. A. *Macromolecules* **2009**, *42*, 2317−2320.
(32) Chueh, C.-C.; Higashihara, T.; Tsai, J.-H.; Ueda, M.; Chen, W.-C. *Org. Electron.* **2009**, *10*, 1541−1548.
(33) Yokozawa, T.; Suzuki, R.; Nojima, M.; Ohta, Y.; Yokoyama, A. *Macromol. Rapid Commun.* **2011**, *32*, 801−806.
(34) Yokozawa, T.; Adachi, I.; Miyakoshi, R.; Yokoyama, A. *High Perform. Polym.* **2007**, *19*, 684−699.
(35) Lin, Y.-H.; Smith, K. A.; Kempf, C. N.; Verduzco, R. *Polym. Chem.* **2013**, *4*, 229.
(36) Sommer, M.; Komber, H.; Huettner, S.; Mulherin, R.; Kohn, P.; Greenham, N. C.; Huck, W. T. S. *Macromolecules* **2012**, *45*, 4142−4151.
(37) Tao, Y.; McCulloch, B.; Kim, S.; Segalman, R. A. *Soft Matter* **2009**, *5*, 4219.
(38) Kamps, A. C.; Fryd, M.; Park, S.-J. *ACS Nano* **2012**, *6*, 2844−2852.
(39) Benanti, T. L.; Kalaydjian, A.; Venkataraman, D. *Macromolecules* **2008**, *41*, 8312−8315.
(40) Urien, M.; Erothu, H.; Cloutet, E.; Hiorns, R. C.; Vignau, L.; Cramail, H. *Macromolecules* **2008**, *41*, 7033−7040.
(41) Wu, Z.-Q.; Ono, R. J.; Chen, Z.; Li, Z.; Bielawski, C. W. *Polym. Chem.* **2011**, *2*, 300.
(42) Smeets, A.; Willot, P.; De Winter, J.; Gerbaux, P.; Verbiest, T.; Koeckelberghs, G. *Macromolecules* **2011**, *44*, 6017−6025.
(43) Zhang, C.; Choi, S.; Haliburton, J.; Cleveland, T.; Li, R.; Sun, S.-S.; Ledbetter, A.; Bonner, C. E. *Macromolecules* **2006**, *39*, 4317−4326.
(44) Sun, S.-S.; Zhang, C.; Ledbetter, A.; Choi, S.; Seo, K.; Bonner, C. E.; Drees, M.; Sariciftci, N. S. *Appl. Phys. Lett.* **2007**, *90*, 043117−043117−3.
(45) Jeffries-El, M.; Sauvé, G.; McCullough, R. D. *Macromolecules* **2005**, *38*, 10346−10352.
(46) Li, Z.; Ono, R. J.; Wu, Z.-Q.; Bielawski, C. W. *Chem. Commun.* **2011**, *47*, 197.
(47) Wu, W.-C.; Tian, Y.; Chen, C.-Y.; Lee, C.-S.; Sheng, Y.-J.; Chen, W.-C. *Langmuir* **2007**, *23*, 2805−2814.
(48) Marsitzky, D.; Klapper, M.; Müllen, K. *Macromolecules* **1999**, *32*, 8685−8688.
(49) Yokoyama, A.; Suzuki, H.; Kubota, Y.; Ohuchi, K.; Higashimura, H.; Yokozawa, T. *J. Am. Chem. Soc.* **2007**, *129*, 7236−7237.
(50) Kline, R. J.; McGehee, M. D.; Kadnikova, E. N.; Liu, J.; Fréchet, J. M. J.; Toney, M. F. *Macromolecules* **2005**, *38*, 3312−3319.
(51) Sirringhaus, H.; Brown, P. J.; Friend, R. H.; Nielsen, M. M.; Bechgaard, K.; Langeveld-Voss, B. M. W.; Spiering, A. J. H.; Janssen, R. a. J.; Meijer, E. W.; Herwig, P.; de Leeuw, D. M. *Nature* **1999**, *401*, 685−688.
(52) Verploegen, E.; Mondal, R.; Bettinger, C. J.; Sok, S.; Toney, M. F.; Bao, Z. *Adv. Funct. Mater.* **2010**, *20*, 3519−3529.
(53) Hammond, M. R.; Kline, R. J.; Herzing, A. A.; Richter, L. J.; Germack, D. S.; Ro, H.-W.; Soles, C. L.; Fischer, D. A.; Xu, T.; Yu, L.; Toney, M. F.; DeLongchamp, D. M. *ACS Nano* **2011**, *5*, 8248−8257.
(54) Chen, W.; Xu, T.; He, F.; Wang, W.; Wang, C.; Strzalka, J.; Liu, Y.; Wen, J.; Miller, D. J.; Chen, J.; Hong, K.; Yu, L.; Darling, S. B. *Nano Lett.* **2011**, *11*, 3707−3713.
(55) Beiley, Z. M.; Hoke, E. T.; Noriega, R.; Dacuña, J.; Burkhard, G. F.; Bartelt, J. A.; Salleo, A.; Toney, M. F.; McGehee, M. D. *Adv. Energy Mater.* **2011**, *1*, 954−962.
(56) Chen, S. H.; Chou, H. L.; Su, A. C.; Chen, S. A. *Macromolecules* **2004**, *37*, 6833−6838.
(57) Grell, M.; Bradley, D. D. C.; Ungar, G.; Hill, J.; Whitehead, K. S. *Macromolecules* **1999**, *32*, 5810−5817.
(58) Myers, S. B.; Register, R. A. *Macromolecules* **2008**, *41*, 6773−6779.
(59) Gan, Z.; Jiang, B.; Zhang, J. *J. Appl. Polym. Sci.* **1996**, *59*, 961−967.
(60) Lin, M.-C.; Wang, Y.-C.; Chen, J.-H.; Chen, H.-L.; Müller, A. J.; Su, C.-J.; Jeng, U.-S. *Macromolecules* **2011**, *44*, 6875−6884.
(61) Takeshita, H.; Fukumoto, K.; Ohnishi, T.; Ohkubo, T.; Miya, M.; Takenaka, K.; Shiomi, T. *Polymer* **2006**, *47*, 8210−8218.
(62) Loo, Y.-L.; Register, R. A.; Ryan, A. J. *Macromolecules* **2002**, *35*, 2365−2374.
(63) Iovu, M. C.; Craley, C. R.; Jeffries-EL, M.; Krankowski, A. B.; Zhang, R.; Kowalewski, T.; McCullough, R. D. *Macromolecules* **2007**, *40*, 4733−4735.
(64) Iovu, M. C.; Jeffries-El, M.; Zhang, R.; Kowalewski, T.; McCullough, R. D. *J. Macromol. Sci., Part A* **2006**, *43*, 1991−2000.
(65) Higashihara, T.; Ohshimizu, K.; Hirao, A.; Ueda, M. *Macromolecules* **2008**, *41*, 9505−9507.
(66) Ho, V.; Boudouris, B. W.; McCulloch, B. L.; Shuttle, C. G.; Burkhardt, M.; Chabinyc, M. L.; Segalman, R. A. *J. Am. Chem. Soc.* **2011**, *133*, 9270−9273.

(67) Marat, K. SpinWorks is available for download: http://www.columbia.edu/cu/chemistry/groups/nmr/SpinWorks.html.
(68) Pasch, H.; Schrepp, W. *MALDI-TOF Mass Spectrometry of Synthetic Polymers*; Springer: Berlin, 2003.
(69) Jiang, Z.; Li, X.; Strzalka, J.; Sprung, M.; Sun, T.; Sandy, A. R.; Narayanan, S.; Lee, D. R.; Wang, J. *J. Synchrotron Radiat.* **2012**, *19*, 627−636.
(70) Jiang, Z. GIXSGUI is available for download: http://www.aps.anl.gov/Sectors/Sector8/Operations/GIXSGUI.html.
(71) Loewe, R. S.; Ewbank, P. C.; Liu, J.; Zhai, L.; McCullough, R. D. *Macromolecules* **2001**, *34*, 4324−4333.
(72) Zhang, X.; Tian, H.; Liu, Q.; Wang, L.; Geng, Y.; Wang, F. *J. Org. Chem.* **2006**, *71*, 4332−4335.
(73) Dyke, J. M.; Groves, A. P.; Morris, A.; Ogden, J. S.; Dias, A. A.; Oliveira, A. M. S.; Costa, M. L.; Barros, M. T.; Cabral, M. H.; Moutinho, A. M. C. *J. Am. Chem. Soc.* **1997**, *119*, 6883−6887.